

Detection of  $C_2H_4$  in Neptune from ISO/PHT-S observationsB. Schulz<sup>1</sup>, Th. Encrenaz<sup>2</sup>, B. Bézard<sup>2</sup>, P. N. Romani<sup>3</sup>, E. Lellouch<sup>2</sup>, and S. K. Atreya<sup>4</sup><sup>1</sup> ISO Data Centre, ESA, PO box 50727, E-28080 Madrid<sup>2</sup> DESPA, Observatoire de Paris, F-92195 Meudon, France<sup>3</sup> NASA Goddard Space Flight Center, Code 693.2, Greenbelt, MD 20771, USA<sup>4</sup> The University of Michigan, Ann Arbor, MI 48109-1243, USA

Received 26 July 1999 / Accepted

**Abstract.** The 6–12  $\mu\text{m}$  spectrum of Neptune has been recorded with the PHT-S instrument of the Infrared Space Observatory (ISO) at a resolution of 0.095  $\mu\text{m}$ . In addition to the emissions of  $CH_4$ ,  $CH_3D$  and  $C_2H_6$  previously identified, the spectrum shows the first firm identification of ethylene  $C_2H_4$ . The inferred column density above the 0.2-mbar level is in the range  $(1.1\text{--}3)\times 10^{14}$  molecules  $\text{cm}^{-2}$ . To produce this low amount, previous photochemical models invoked rapid mixing between the source and sink regions of  $C_2H_4$ . We show that this requirement can be relaxed if recent laboratory measurements of  $CH_4$  photolysis branching ratios at Lyman  $\alpha$  are used.

**Key words:** Planets and satellites – Neptune – Infrared: solar system

## 1. Introduction

In the stratospheres of all giant planets, methane ( $CH_4$ ) photochemistry leads to the formation of many hydrocarbons. Photochemical models have been developed by several authors (e.g. Gladstone et al. 1996 for Jupiter, Moses et al. 1999 for Saturn, Atreya et al. 1991 for Uranus, and Romani et al. 1993 for Neptune) to account for the observations of the detected hydrocarbons ( $C_2H_2$  and  $C_2H_6$ ) and to predict the abundances of minor species. Among the expected products in significant amount is ethylene ( $C_2H_4$ ). This compound however was only detected in the northern auroral region of Jupiter, from emission in the  $\nu_7$  band at 10.5  $\mu\text{m}$  observed in Voyager/IRIS spectra (Kim et al. 1985). On Neptune, a tentative detection of the same band of ethylene was presented by Orton et al. (1987) from ground-based low-resolution spectral measurements.

Observations with the short-wavelength spectrometer (SWS) of the Infrared Space Observatory (ISO) have led to the detection of several new hydrocarbons in Saturn ( $C_3H_4$ ,  $C_4H_2$ , and  $CH_3$ ; de Graauw et al. 1997; Bézard et al. 1998) and Neptune ( $CH_3$ ; Bézard et al. 1999b). In the

case of Neptune, the 7–14  $\mu\text{m}$  SWS spectrum, recorded at a spectral resolution of 0.005  $\mu\text{m}$  has been studied by Bézard (1998). Information was retrieved upon the stratospheric temperature, the  $CH_4$  stratospheric mixing ratio, and the  $C_2H_2$  and  $C_2H_6$  abundance profiles. In the case of  $C_2H_4$ , only an upper limit of its stratospheric column abundance ( $8\times 10^{14}$  molecules  $\text{cm}^{-2}$  above the 0.2-mbar level) was inferred (Bézard et al. 1999a).

We present in this paper the 6–12  $\mu\text{m}$  spectrum of Neptune recorded with another ISO instrument, ISOPHOT, and we report the first firm detection of  $C_2H_4$  on Neptune. Section 2 describes the observations and the data reduction. Section 3 presents the modelling and the determination of the  $C_2H_4$  abundance. Results are discussed in Section 4 and conclusions are presented in Section 5.

## 2. Observations and data reduction

The photometer ISOPHOT (Lemke et al. 1996) of ISO (Kessler et al. 1996) included a subsystem (PHT-S) made of two grating spectrometers operating at 2.5–5  $\mu\text{m}$  (SS) and 6–12  $\mu\text{m}$  (SL) with a spectral resolution of 0.0445  $\mu\text{m}$  and 0.0949  $\mu\text{m}$  respectively (Klaas et al. 1997). The two spectra were simultaneously recorded on the two linear arrays of 64 elements Si:Ga detectors each. The entrance aperture was  $24''\times 24''$ .

The PHT-S spectrum of Neptune was recorded on May 8, 1997, between 3:41 UT and 12:29 UT. The diameter of Neptune was then 2.25'', and the sub-Earth latitude was  $-30.6^\circ$ . Twelve pairs of spectra, of 1024 sec integration time each, were successively recorded on and off the source (with the offset position at 5' north), in order to subtract the sky background.

The data reduction was performed using the PHT Interactive Analysis software package PIA V7.3.2(e) (Gabriel et al. 1997) together with IDL routines that facilitate individual inspection of the signals and deglitching. The Si:Ga photoconductors, arranged in two arrays of 64 pixels each, exhibit transients of the photocurrent after a flux change. This behavior impacts the deglitching procedure as well as the assignment of flux densities.

Send offprint requests to: B. Schulz (bschulz@iso.vilspa.esa.es)

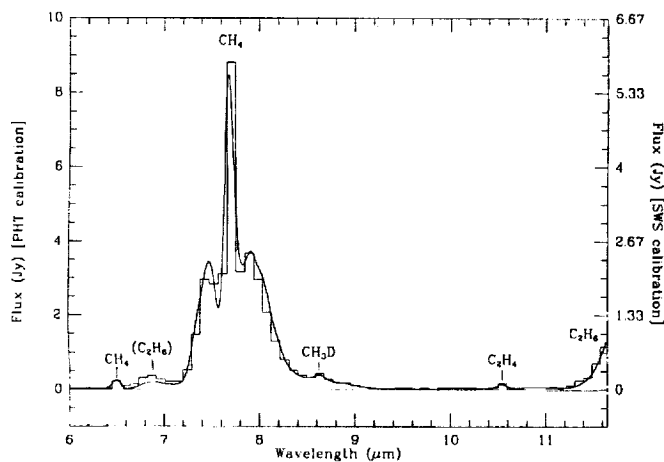


**Fig. 1.** PHT-S spectrum of Neptune observed in the 6–11.6  $\mu\text{m}$  range. Emission features from  $\text{CH}_4$ ,  $\text{CH}_3\text{D}$ ,  $\text{C}_2\text{H}_6$  and  $\text{C}_2\text{H}_4$  are clearly detected. The flux scale on the left axis corresponds to the direct PHT-S calibration, that on the right axis to a rescaling of the data by a factor of 0.67 to agree with the SWS observations of the 7.7- $\mu\text{m}$   $\text{CH}_4$  band.

The 32 s integration ramps with 128 readouts were divided into 16 subramps. The fitted slopes  $s(t)$ , being a measure of the photo current, were deglitched automatically using an algorithm that clips all values where  $|s(t) - b(t)| > 3.5\sigma$ .  $b(t)$  are the boxcar smoothed slopes with the smoothing parameter tuned to follow the slow transients of the photo current with time  $t$ .  $\sigma$  is calculated as  $\sqrt{\sum (s(t) - b(t))^2 / (n - 1)}$ , where  $n$  is the number of slopes.

The assignment of flux densities was performed using the new dynamic calibration method (Acosta-Pulido 1999). It is based on the reproducibility of the transient behavior when a given detector pixel is exposed to similar flux levels. The method, which is implemented into PIA, requires the prior subtraction of the exposure time-dependent dark current. The transients also differ from pixel to pixel, so PIA contains a database for all pixels of measured transients with 27 calibration sources, covering most of the accessible flux range. After deriving 12 spectra on source and 12 on the background, we concatenated the pairwise differences within PIA and then averaged each pixel to derive the final flux density.

The uncertainties in the PIA results and propagated statistical errors are usually smaller than the variations due to long-term responsivity changes and transient repeatability. Consistency checks within the database of transients suggest average accuracies of 10 to 15% over all pixels. This is also consistent with results from long-term stability checks (Schulz 1999) which give 10%. Relative uncertainties between fluxes of adjacent detector pixels with similar flux levels are smaller, i.e. closer to the statistical errors. The error in the SED models of the calibration standards is not included and ranges between 3 and 5%.

Fig. 1 shows the PHT-S spectrum of Neptune between 6 and 12  $\mu\text{m}$ . The 1- $\sigma$  noise level is estimated to about 0.010 Jy at 6–7  $\mu\text{m}$  and 0.020 Jy at 10–11  $\mu\text{m}$ . The spectrum is dominated by the strong  $\nu_4$  band of  $\text{CH}_4$  which peaks at 7.7  $\mu\text{m}$ .  $\text{CH}_4$  emission is also seen in the Q-branch of the weak  $\nu_2$  band at 6.5  $\mu\text{m}$ , observed here for the first time.  $\text{CH}_3\text{D}$  is detected at 8.6  $\mu\text{m}$  through its  $\nu_6$  band and contributes with its  $\nu_5$  band to the emission at 6.8  $\mu\text{m}$ . The wing of the  $\nu_9$  band of  $\text{C}_2\text{H}_6$  is visible beyond 11.4  $\mu\text{m}$ . All these emissions above 7  $\mu\text{m}$  were previously detected in the SWS spectrum of Neptune (Bézard 1998). In addition, the PHT-S spectrum of Neptune shows a new emission feature in a single pixel, at 10.5  $\mu\text{m}$ , at a level of 0.1 Jy, i.e. 5 times above the noise level. We attribute this 10.5  $\mu\text{m}$  emission to the Q-branch of the  $\text{C}_2\text{H}_4$   $\nu_7$  band, which is centered at 949  $\text{cm}^{-1}$  (10.53  $\mu\text{m}$ ).

The comparison of the PHT-S and SWS data shows a very good agreement in the shapes of the two spectra, but a difference in the absolute calibration scale by a factor of 1.5, the PHT-S fluxes being higher than the SWS ones. The two scales are indicated on Fig. 1. We have presently no explanation for this discrepancy.

In this paper, we modelled the observations with the “nominal” atmospheric model (methane and temperature profiles) derived by Bézard (1998) from an analysis of the SWS spectrum between 7 and 14  $\mu\text{m}$  (see Section 3). The  $\text{C}_2\text{H}_2$  and  $\text{C}_2\text{H}_6$  abundances inferred from this model were in very good agreement with previous results from Voyager data (Bézard et al. 1991) and ground-based infrared measurements (Orton et al. 1987). For consistency, we used here the SWS calibration of the PHT-S data to infer the “nominal”  $\text{C}_2\text{H}_4$  abundance, but we took into account the difference in the two instrument calibrations in the error analysis.

### 3. Radiative transfer analysis

Synthetic spectra were generated from a line-by-line radiative transfer program that includes the  $\text{H}_2$ -He collision-induced absorption and molecular opacity from  $\text{CH}_4$ ,  $\text{CH}_3\text{D}$ ,  $\text{C}_2\text{H}_6$ , and  $\text{C}_2\text{H}_4$ . Line parameters come from the 1997 spectroscopic Geisa databank (Jacquinot-Husson et al. 1997). We used the same temperature profile as in Bézard (1998) and Bézard et al. (1999b).  $\text{C}_2\text{H}_4$  spectral calculations were carried out assuming LTE at all atmospheric levels.

To derive constraints on the  $\text{C}_2\text{H}_4$  stratospheric column abundance, we proceeded as did Bézard et al. in their analysis of the methyl radical emission. We considered vertical profiles derived from photochemical calculations, allowing for the uncertainty in the photochemical scheme (Profiles 1–5 in Table 1) and in the eddy mixing profile (Profiles 6–7) (see Section 4). To determine the  $\text{C}_2\text{H}_4$  abundance implied by the observations, we then multiplied each test profile by a constant factor that allowed us to best reproduce the intensity of the observed 10.5- $\mu\text{m}$

emission in a least-squares sense. We found column densities for these rescaled profiles in the range  $1.7\text{--}2.2 \times 10^{14}$  molecules  $\text{cm}^{-2}$  down to the 0.2-mbar level (Table 1). The C<sub>2</sub>H<sub>4</sub> abundance below this level does not contribute significantly to the emission, being located at colder levels in the stratosphere.

The spectrum generated with our nominal model (Profile 5 for C<sub>2</sub>H<sub>4</sub>) is shown in Fig. 1 in the whole range 6–11.6  $\mu\text{m}$ . The discrepancy between the synthetic and observed spectra around 6.8  $\mu\text{m}$  may be due to the presence of the  $\nu_8$  band of C<sub>2</sub>H<sub>6</sub>. This band was not included in the calculations as no line compilation exists in the usual spectral databanks. In the other regions, the agreement is quite satisfactory. Spectra incorporating various vertical profiles of C<sub>2</sub>H<sub>4</sub> (Profiles 1–5, Fig. 2) are shown in Fig. 3 (see Section 4 for a full description of the profiles).

Our nominal value for the inferred column density is  $1.7 \times 10^{14}$  molecules  $\text{cm}^{-2}$ , using the rescaled profile 5. Uncertainties arise from the noise level ( $\pm 20\%$ ), the flux calibration of the ISO spectrum, the model temperature profile, and the C<sub>2</sub>H<sub>4</sub> vertical profile. For the flux calibration uncertainty, we assumed a  $+50\%$  error interval that includes the PHT-S flux scale. Uncertainties from the temperature profile were estimated using the extreme “cool” and “warm” profiles from Bézard et al. (1999b). A  $+20\%$  error range was then obtained. Finally the uncertainty due to the C<sub>2</sub>H<sub>4</sub> height profile is  $\pm 25\%$  (Table 1). Combining the above error bars, we conclude that the C<sub>2</sub>H<sub>4</sub> column density above the 0.2-mbar level is in the range  $(1.1\text{--}3) \times 10^{14}$  molecules  $\text{cm}^{-2}$ .

#### 4. Comparison with photochemical models

Photochemical calculations were carried out with a one-dimensional model as in Bézard et al. (1999b). The model has been most recently described in Bishop et al. (1997). Chemical reactions and kinetic rates included in the modeling are listed in Table 3 of Bishop et al. with minor updates since then, except for the methane photolysis branching ratios at Lyman  $\alpha$  and the rate coefficient for  $\text{C}_2\text{H}_4 + \text{H} + \text{M} \rightarrow \text{C}_2\text{H}_5 + \text{M}$ , which are both discussed below. Photolysis rates are calculated for disk-averaged conditions, and account for both solar irradiance and the Lyman  $\alpha$  skyglow from the local interstellar medium. Solar minimum conditions, representative of the time of the ISO observations, were used, because the chemical lifetime of C<sub>2</sub>H<sub>4</sub> was found to be shorter than the solar cycle. We used a CH<sub>4</sub> mole fraction equal to  $1.4 \times 10^{-3}$  in the lower stratosphere as favored by observations of the  $\nu_4$  band of methane by ISO (Bézard 1998). The model incorporates a downward flux of atomic hydrogen at the upper boundary equal to  $4 \times 10^7 \text{ cm}^{-2}\text{s}^{-1}$ , representing H production from solar EUV at solar minimum.

We used as “nominal” an eddy mixing coefficient,  $K$ , proportional to the atmospheric number density  $n$  to the  $-0.6$  power, and equal to  $K_h = 10^7 \text{ cm}^2\text{s}^{-1}$  at the methane

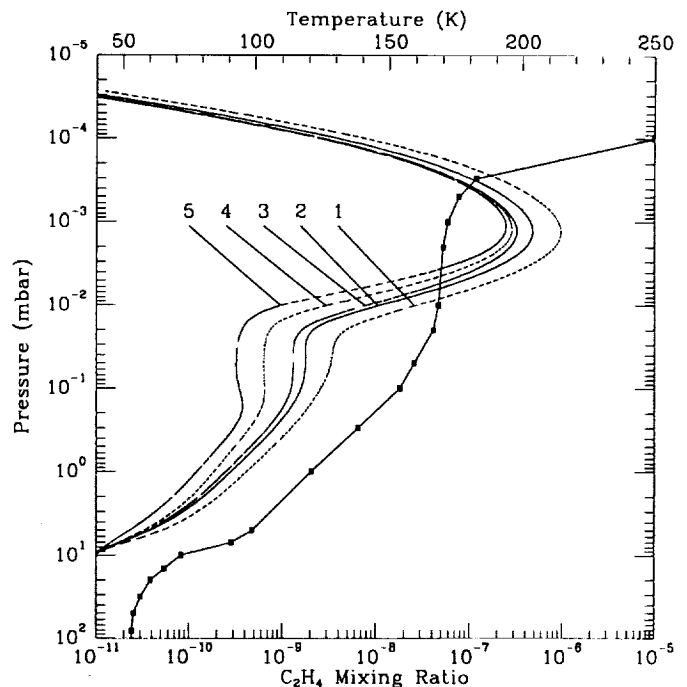


Fig. 2. Temperature-pressure profile used in the radiative transfer analysis (solid line with dots, top axis) and calculated C<sub>2</sub>H<sub>4</sub> profiles. Three different CH<sub>4</sub> photolysis branching ratios at Lyman  $\alpha$  were first used: Romani (1996) [long-dashed line], Heck et al. (1996) [dash-dot line], Smith and Raulin (1999) [solid line], all with the nominal value of the reaction rate coefficient for  $\text{H} + \text{C}_2\text{H}_4$  from Lightfoot and Pilling (1987). Different expressions of the reaction rate coefficient of  $\text{H} + \text{C}_2\text{H}_4$  were also considered: Lightfoot and Pilling’s (1987) nominal expression [solid line], Lightfoot and Pilling’s fast rate [short-dashed line], Baulch et al. (1994) [dotted line], all with CH<sub>4</sub> photolysis branching ratios from Smith and Raulin (1999).

homopause. This type of  $K$  profile was shown to be compatible with the ISO observations of CH<sub>3</sub> if the low pressure rate coefficient for the methyl self-reaction was between that of Slagle et al. (1988) and Macpherson et al. (1985). Following Bézard et al. (1999b), we also varied the  $K$  profile, considering constraints from other observations of Neptune hydrocarbons (Bishop et al. 1997).

Ethylene photochemistry is similar to that of the methyl radical CH<sub>3</sub> (see Bézard et al. 1999b). It has a source high in the stratosphere (3 to 0.3  $\mu\text{bar}$  region) from methane photolysis, a three-body sink low in the stratosphere (0.1 to 1 mbar region), and transport connecting the two. Methylidyne (CH) is directly produced from methane photolysis as is methyl, and yields ethylene via  $\text{CH} + \text{CH}_4$ . Triplet methylene ( $^3\text{CH}_2$ ), another product of methane photolysis, also leads to C<sub>2</sub>H<sub>4</sub> formation. The net effect is that C<sub>2</sub>H<sub>4</sub> production is sensitive to the sum of the photolysis pathways that yield either  $^3\text{CH}_2$  or CH. The dominant sink for ethylene is, in the lower stratosphere, the three-body reaction  $\text{C}_2\text{H}_4 + \text{H} + \text{M} \rightarrow \text{C}_2\text{H}_5 + \text{M}$ . The C<sub>2</sub>H<sub>4</sub> column density is proportional to its

production rate but inversely proportional to the loss rate coefficient and to the transport rate between the source and the sink.

The methane photolysis rate is dominated by the flux at Lyman  $\alpha$ . Unfortunately, the branching ratios for the possible pathways at Lyman  $\alpha$  are still not known. Furthermore, there are disagreements among the laboratory experiments about the relative importance of the different pathways and the quantum yield of H and H<sub>2</sub> in methane photolysis (Smith and Raulin 1999, Brownsword et al. 1997, Heck et al. 1996, Mordaunt et al. 1993). We first used the same branching ratios as in Romani (1996) (Profile 1 in Fig. 2). These branching ratios are based upon the work of Mordaunt et al. (1993) and previous work. As can be seen in Fig. 3, this produces too large a column density of C<sub>2</sub>H<sub>4</sub> to be compatible with the observations. We next tried the branching ratios suggested by Heck et al. (1996) (Profile 2). The main difference with those of Romani (1996) is that the production of <sup>3</sup>CH<sub>2</sub> + 2H is reduced from 0.21 to zero while the production of CH<sub>3</sub> + H is increased by a similar amount. The column density of C<sub>2</sub>H<sub>4</sub> decreases, but not enough to match the observations (see Table 1 and Fig. 3). Lastly we used the branching ratios of Smith and Raulin (1999) (Profile 3), which are very similar to those of Brownsword et al. (1997). With respect to ethylene formation, the major difference between these branching ratios and those of Heck et al. (1996) is a reduction in the branching ratio to form CH + H<sub>2</sub> + H from 0.11 to 0.06. The modelled C<sub>2</sub>H<sub>4</sub> column density is now close to the value derived from the observations.

The predicted C<sub>2</sub>H<sub>4</sub> emission is still slightly too high, although the branching ratios of Smith and Raulin result in the lowest model predicted C<sub>2</sub>H<sub>4</sub> column density of all that we tried. We next investigated the loss processes for ethylene. We used the “fast” rate coefficient for H + C<sub>2</sub>H<sub>4</sub> from Lightfoot and Pilling (1987) (the largest possible rate coefficient within their reported error bars) (Profile 4). Using this rate coefficient with the Smith and Raulin branching ratios, the modelled C<sub>2</sub>H<sub>4</sub> profile now yields the correct abundance to reproduce the observed emission within the noise level (see Table 1, Figs. 2–3). It can be noted that the rate coefficient expression suggested by Baulch et al. (1994) for this reaction is faster than the “fast” Lightfoot and Pilling (1987) value. It results in a predicted C<sub>2</sub>H<sub>4</sub> emission still consistent with the observations (Profile 5).

It is also possible to reduce the C<sub>2</sub>H<sub>4</sub> column density by changing K. A first way is to keep the same functional form,  $K \sim n^{-0.6}$ , but to decrease its value at the methane homopause. Methane photolysis then occurs at higher number densities, closer to the C<sub>2</sub>H<sub>4</sub> loss region. To reproduce the C<sub>2</sub>H<sub>4</sub> emission feature with the Smith and Raulin (1999) branching ratios K must be lowered to  $5 \times 10^6 \text{ cm}^2 \text{ s}^{-1}$  at the methane homopause, but with the Romani (1996) branching ratios K must be decreased below  $10^6 \text{ cm}^2 \text{ s}^{-1}$ . The former value is within the bounds

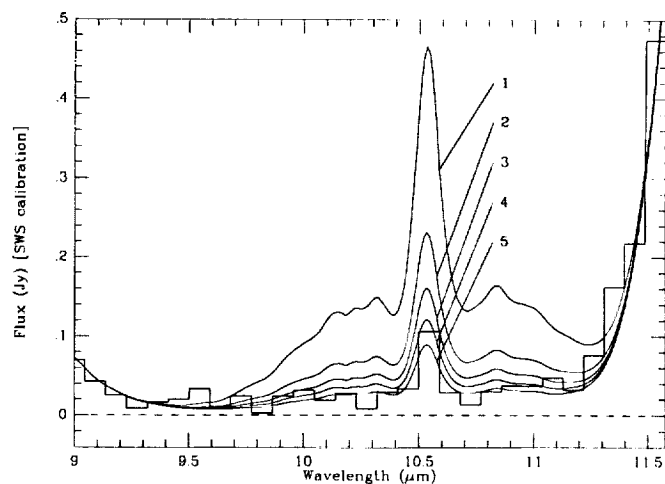


Fig. 3. Synthetic spectra calculated with the C<sub>2</sub>H<sub>4</sub> profiles 1–5 of Table 1 (solid lines), displayed in Fig. 2, are compared with the PHT-S spectrum in the region of the  $\nu_7$  ethylene band (histograms).

permitted by the ISO/SWS CH<sub>3</sub> observations while the latter is not (Bézard et al. 1999b). A second way is to alter the form of K to increase the downward transport of C<sub>2</sub>H<sub>4</sub> from its source to sink. This was done previously by Romani et al. (1993) and Bishop et al. (1997). They found that the model predicted C<sub>2</sub>H<sub>4</sub> with  $K \sim n^{-0.6}$  was too high for the Voyager UVIS solar occultation light curves (note that these papers were prior to Brownsword et al. (1997) and thus had high C<sub>2</sub>H<sub>4</sub> production). They solved the problem by increasing the transport rate between the  $\mu\text{bar}$  and mbar region (type “B” eddy profile in Romani et al. 1993) and using the fast rate coefficient for H + C<sub>2</sub>H<sub>4</sub> from Lightfoot and Pilling. With this combination of transport and chemistry, the C<sub>2</sub>H<sub>4</sub> column density is now within the range allowed by ISOPHOT although at the upper bounds.

## 5. Summary and conclusions

The PHT-S detection of the C<sub>2</sub>H<sub>4</sub>  $\nu_7$  band on Neptune implies a column density equal to  $1.7^{+1.3}_{-0.6} \times 10^{14} \text{ molecules cm}^{-2}$ . This result is fully consistent with the upper limit of  $8 \times 10^{14} \text{ molecules cm}^{-2}$  reported by Bézard et al. (1999a) from ISO-SWS observations. Orton et al.’s (1987) observations of Neptune at a resolution of  $0.23 \mu\text{m}$  showed enhanced emission around  $10.5 \mu\text{m}$  that was attributed to C<sub>2</sub>H<sub>4</sub>. Their reported brightness temperature at  $10.5 \mu\text{m}$  corresponds to a  $0.06 \text{ Jy}$  flux ( $\pm 20\%$ ), in good agreement with the PHT-S spectrum which yields a value of  $0.09$  (PHT calibration) or  $0.06 \text{ Jy}$  (SWS calibration) after convolution at  $0.23\text{-}\mu\text{m}$  resolution.

For the photochemical model to reproduce both the ISO CH<sub>3</sub> and C<sub>2</sub>H<sub>4</sub> emission features with  $K \sim n^{-0.6}$ , the CH<sub>4</sub> photolysis branching ratios at Lyman  $\alpha$  must be similar to those proposed by Brownsword et al. (1997)

Table 1. Comparison of photochemical models to ISO observations

Model	$K_h$ (cm <sup>2</sup> s <sup>-1</sup> )	CH <sub>4</sub> branching ratios at Ly $\alpha$	H + C <sub>2</sub> H <sub>4</sub> rate coefficient	Model C <sub>2</sub> H <sub>4</sub> (molecules cm <sup>-2</sup> at 0.2 mbar)	Scaled C <sub>2</sub> H <sub>4</sub> <sup>a</sup> (molecules cm <sup>-2</sup> at 0.2 mbar)
1	1×10 <sup>7</sup>	Romani (1996)	Lightfoot & Pilling (1987) nominal	8.8×10 <sup>14</sup>	1.9×10 <sup>14</sup>
2	1×10 <sup>7</sup>	Heck et al. (1996)	Lightfoot & Pilling (1987) nominal	4.3×10 <sup>14</sup>	1.9×10 <sup>14</sup>
3	1×10 <sup>7</sup>	Smith & Raulin (1999)	Lightfoot & Pilling (1987) nominal	3.0×10 <sup>14</sup>	1.9×10 <sup>14</sup>
4	1×10 <sup>7</sup>	Smith & Raulin (1999)	Lightfoot & Pilling (1987) fast	2.2×10 <sup>14</sup>	1.8×10 <sup>14</sup>
5	1×10 <sup>7</sup>	Smith & Raulin (1999)	Baulch et al. (1994)	1.6×10 <sup>14</sup>	1.7×10 <sup>14</sup>
6	1×10 <sup>6</sup>	Smith & Raulin (1999)	Lightfoot & Pilling (1987) nominal	2.2×10 <sup>14</sup>	2.2×10 <sup>14</sup>
7	5×10 <sup>7</sup>	Smith & Raulin (1999)	Lightfoot & Pilling (1987) nominal	3.3×10 <sup>14</sup>	1.8×10 <sup>14</sup>

<sup>a</sup> Needed to reproduce the C<sub>2</sub>H<sub>4</sub> emission intensity

and Smith and Raulin (1999). Furthermore, if  $K_h = 10^7$  cm<sup>2</sup>s<sup>-1</sup>, the rate coefficient for H + C<sub>2</sub>H<sub>4</sub> must be near the “fast” value of Lightfoot and Pilling (1987).

It is also possible to invoke rapid transport between the  $\mu$ bar and mbar region (type “B” K profile from Romani et al. 1993). In this case, the CH<sub>4</sub> photolysis branching ratios at Lyman  $\alpha$  that lead to C<sub>2</sub>H<sub>4</sub> production must be increased above those proposed by Brownsword et al. (1997) and Smith and Raulin (1999). However, a fast rate for H + C<sub>2</sub>H<sub>4</sub> is still needed.

In summary, previous photochemical models required rapid transport and a fast sink for C<sub>2</sub>H<sub>4</sub> to reproduce observations. Now the new laboratory measurements of CH<sub>4</sub> photolysis branching ratios at Lyman  $\alpha$  allow us to relax that requirement. The need for laboratory measurements mentioned by Romani et al. (1993) — the CH<sub>4</sub> branching ratios at Lyman  $\alpha$ , and the rate coefficient of H + C<sub>2</sub>H<sub>4</sub> at low temperatures and pressures — is still present.

**Acknowledgements.** ISO is an ESA project with instruments funded by ESA Member States (especially the PI countries: France, Germany, the Netherlands and the United Kingdom) and with the participation of NASA and ISAS. The PHT instrument (PI: D. Lemke) has been developed at MPIA.

## References

- Acosta-Pulido J., 1999, Dynamic Calibration of ISOPHOT-S, IDC technical note, in preparation
- Atreya S.K., Sandel B.R., Romani P.N., 1991, Photochemistry and vertical mixing. In: Bergstrahl J.T., Miner E.D., Matthews M.S. (eds) Uranus. Univ. Arizona Press, Tucson, p.110
- Baulch D.L., Cobos C.J., Cox R.A., et al., 1994, J. Phys. Chem. Ref. Data 23, 847
- Bézard B., 1998, Ann. Geophys. 16 (Suppl. III), C1037
- Bézard B., Romani P.N., Conrath B.J., Maguire W.C., 1991, JGR 96, 18961
- Bézard B., Feuchtgruber H., Moses J.I., Encrenaz T., 1998, A&A 334, L41
- Bézard B., Feuchtgruber H., Encrenaz T., 1999a, ESA-SP 427, 153
- Bézard B., Romani P.N., Feuchtgruber H., Encrenaz T., 1999b, ApJ 515, 868
- Bishop J., Romani P.N., Atreya S.K., 1997, Plan. Space Sci. 46, 1
- Brownsword R.A., Hillenkamp M., Laurent T., Vasta R.K., Volpp H.R., Wolfrum J., 1997, Chem. Phys. Lett. 266, 259
- de Graauw Th., Feuchtgruber H., Bézard B., et al., 1997, A&A 321, L13
- Gabriel C., et al., 1997, In: Hunt G., Payne H.E. (eds) Proc. ADASS VI conference, ASP Conf. Ser. 125, p.108
- Gladstone G.R., Allen M., Yung Y.L., 1996, Icarus 119, 1
- Heck A.J.R., Zare R.N., Chandler D.W., 1996, J. Chem. Phys. 104, 4019
- Jacquinet-Husson N., Arié E., Ballard J., et al., 1997, JQSRT 62, 205
- Kim S.J., Caldwell J., Rivolo A. R., Wagener R., Orton G. S., 1985, Icarus 64, 233
- Kessler M.F., Steinz J.A., Anderegg M.E., et al., 1996, A&A 315, L27
- Klaas U., Acosta-Pulido J.A., Ábrahám P., et al., 1997, ESA SP-419, 113
- Lemke D., Klaas U., et al., 1996 A&A 315, L64
- Lightfoot P.D., Pilling M.J., 1987, J. Phys. Chem. 91, 3373
- MacPherson M.T., Pilling M.J., Smith M.J.C., 1985, J. Phys. Chem. 89, 2268
- Mordaunt D.H., Lambert I.R., Morley G.P., et al., 1993, J. Chem. Phys. 98, 2054
- Moses J., Bézard B., Lellouch E., Gladstone G.R., Feuchtgruber H., Allen M., 1999, Icarus, submitted
- Orton G., Aitken D.K., Smith C., Roche P., Caldwell J., Snyder R., 1987, Icarus 70, 1
- Romani P.N., 1996, Icarus 122, 233
- Romani P.N., Bishop J., Bézard B., Atreya S.K., 1993, Icarus 106, 442
- Schulz B., 1999, Long Term Responsivity Stability of ISOPHOT-S, IDC technical note
- Slagle I.R., Gutman D., Davies J.W., Pilling M.J., 1988, J. Phys. Chem. 92, 2455
- Smith N.S., Raulin F., 1999, JGR 104, 1873